Lithos 334–335 (2019) 180–189

Contents lists available at ScienceDirect

Lithos

journal homepage: www.elsevier.com/locate/lithos

Boron isotope variations of Franciscan serpentinites, northern California

Chinatsu Yamada [a,*], Tatsuki Tsujimori [b], Qing Chang [c], Jun-Ichi Kimura [c]

[a] Department of Earth Science, Graduate School of Science, Tohoku University, Aoba, Sendai 980-8578, Japan
[b] Center for Northeast Asian Studies, Tohoku University, Aoba, Sendai 980-8576, Japan
[c] Department of Solid Earth Geochemistry, Japan Agency for Marine-Earth Science and Technology (JAMSTEC), Yokosuka 237-0061, Japan

ARTICLE INFO

Article history:
Received 15 May 2018
Accepted 9 February 2019
Available online 01 March 2019

Keywords:
Serpentinites
Boron isotope
Franciscan complex
California Coast Ranges

ABSTRACT

Serpentinites and serpentinized mantle peridotites with various tectonic origins occur in the Franciscan Complex of the Northern California Cordillera, USA. Boron isotopes of serpentinites differentiate with fluid-mediated processes, and have great potential for key geologic markers in convergent margins. To understand boron isotope behavior within the Franciscan subduction zone system, we apply a newly developed ablation volume correction (AVC) method for in-situ isotope/elemental analyses using a laser-ablation multiple collector inductively-coupled-plasma mass spectrometry (LA-MC-ICPMS) on seventeen different Franciscan serpentinites (sensu *lato*) collected from eight separate areas. Boron abundances and isotope compositions of the studied serpentinites show large variations B = 1.6–239 $\mu g \cdot g^{-1}$, $\delta^{11}B = -12.0$ to +24.4‰, which allow to discriminate the serpentinites into two groups: (1) a lighter $\delta^{11}B$ of −12.0 to +8.8‰ with a lesser B < ~56 $\mu g \cdot g^{-1}$ and (2) a heavier $\delta^{11}B$ of +7.2 to +24.4‰ with a greater B ~34–239 $\mu g \cdot g^{-1}$. These groups lithologically correspond to the presence or absence of associated blueschist-facies metamorphic rocks, respectively. The blueschist-bearing and/or blueschist-associated serpentinites might have been affected by a deep forearc slab fluids in the depth of > ~2 GPa. Preferential partitioning of ^{11}B into fluids released from the subducted slab at shallow leaves lighter $\delta^{11}B$ in the slab resulting in lighter $\delta^{11}B$ in the deep slab fluids. In contrast, the blueschist-absent serpentinites with heavier $\delta^{11}B$ may have formed at a shallow environment where shallow slab or hydrothermal fluids with heavier ^{11}B were present. Lesser versus greater amounts of B in the deep versus shallow serpentinites are also consistent with the dehydration profile of B from a slab. Our results show the versatility of boron isotopes and composition for identification of the origin of serpentinite in Pacific-type orogenic belts.

1. Introduction

Serpentinite is a H_2O-rich rock that forms at tectonic plate boundaries by hydration of peridotites. In a forearc tectonic setting of the arc-trench system (i.e. subduction zone) and paleosubduction zone of Pacific-type orogenic belts, serpentinites of various petrologic and tectonic origins occur due to dynamic convergent margin processes, such as ophiolite obduction, exhumation of high-pressure metamorphic rocks, subduction channel flow (mélange), serpentinite diapirism, and strike-slip faulting (e.g., Coleman, 1971; Gerya et al., 2002; Scambelluri et al., 2004; Deschamps et al., 2013; Uno and Kriby, 2019). Identification of the origin of serpentinites in Pacific-type orogenic belts (Matsuda and Uyeda, 1971; 'cordilleran-type orogeny' of Dewey and Bird, 1970) is important to reconstruct their subduction settings and eventually to quantify fluid and geochemical fluxes in convergent plate margins. However, once serpentinites are exhumed to the surface, identifications of their origin and tectonic environment become difficult.

Since late 80's, boron isotope geochemistry has been applied to serpentinites of paleo-subduction zone setting worldwide. For example, secondary-ion mass spectrometry (SIMS) of antigorite serpentinite from the Trinity ultramafic body of the Klamath Mountains, California found negative $\delta^{11}B$ values ($\delta^{11}B = -10.4$‰ in average; Peacock and Hervig, 1999). In contrast, whole-rock boron isotope analysis from serpentinite seamounts of Mariana (Benton et al., 2001) showed higher $\delta^{11}B$ values ranging from +5.3 to +25.3‰. The heavier boron signature and the wide variation were interpreted by mixing of seawater ($\delta^{11}B = +39.5$‰; Spivack and Edmond, 1987) and the upwelling pore fluid ($\delta^{11}B \sim +13.0$‰) at a shallow level of the forearc seamounts. Moreover, the boron isotope study of the Erro-Tobbio meta-serpentinites of Western Alps, Italy, revealed a wide variation of $\delta^{11}B$ (from +6.8 to +23.4‰) from the serpentinites of various metamorphic grades (Scambelluri and Tonarini, 2012). The results together with Sr–O–H isotopes led the authors to infer a behavior of slab-released fluids into forearc mantle or the slab-mantle interface where the Erro-Tobbio meta-serpentinites formed. More recently, Martin et al. (2016) characterized two contrasting origins of serpentinite in central Guatemala using boron isotope composition $\delta^{11}B$ determined by both SIMS and laser-ablation multiple collector inductively-coupled-plasma mass spectrometry

* Corresponding author at: Graduate School of Science, Tohoku University, Aoba, Sendai 980-8578, Japan.
E-mail address: chinatsu.yamada.r7@dc.tohoku.ac.jp (C. Yamada).

https://doi.org/10.1016/j.lithos.2019.02.004
0024-4937/

(LA-MC-ICPMS). The serpentinites from the mélange show negative $\delta^{11}B$ values ranging from −14.4 to +9.7‰ in same range as metamorphic blocks (−15.3 to +4.3‰), whereas the serpentinites from the ophiolite display positive $\delta^{11}B$ values (0 to +18‰). They proposed that the tectonic origin of serpentinites in subduction zone can be discriminated based on boron isotopic composition. It has been known that boron is effective to quantify hydrous fluid transfer between the slab and the overlying mantle wedge. Boron is a highly fluid-mobile, light element with two stable isotopes (^{10}B and ^{11}B). In general, ^{11}B is preferentially partitioned into fluids with trigonal coordination, whereas ^{10}B is mainly partitioned into solids with tetrahedral coordination (Konrad-Schmolke and Halama, 2014; Peacock and Hervig, 1999). Therefore, $\delta^{11}B$ decreases with increasing depth because of the strong fractionation of ^{11}B into the fluids (Rayleigh fractionation); the fluid is released by dehydration of hydrous minerals in subducting slab (Peacock and Hervig, 1999) and also progressively lighter $\delta^{11}B$ with increasing dehydration depth (e.g., Marschall et al., 2007; Wunder et al., 2005).

Forearc serpentinites with various petrologic and tectonic origin occur in the Franciscan Complex of the northern California Coast Ranges, for example the Coast Range Ophiolite, serpentine diapir and blocks within metasedimentary mélange units (e.g., Coleman, 1996; Tsujimori et al., 2007; Barnes et al., 2013; Wakabayashi, 2011, 2012, 2017, Uno and Kriby, 2019). What are the boron isotope signatures of the Franciscan serpentinites? Does the boron isotopic composition show regional differences? and/or lithological differences? Can boron isotope ratio be used to distinguish the tectonic setting of the serpentinites? To solve these questions, we analyzed several forearc serpentinites (Ring Mountain, Baker Beach, Communications Hill, Santa Teresa, Edgewood Park, Crystal Spring, Kincaid Road, and New Idria from California) using the ablation volume correction (AVC) LA-MC-ICPMS in-situ analytical technique newly developed by Kimura et al. (2016).

2. Geologic setting

The California Cordillera is a portion of the North American Cordillera (NW America), which includes the Sierra Nevada Mountains and the California Coast Ranges. The Sierra Nevada is a volcanic arc, consisting mainly of Mesozoic arc volcanic rocks and granitic batholiths. In contrast, the Coast Ranges contain a wide variety of rocks of forearc association, including the Franciscan Complex (FRC) and the Coast Range Ophiolite (CRO), which are overlain by forearc basin sediments of the Great Valley Group (e.g., Ernst, 1970, 1975, 2017; Wakabayashi, 1999, 2015, 2017). The mountain building of the Coast Ranges is attributed mainly to the San Andreas Fault, which is a right-lateral strike-slip fault system, juxtaposing the Pacific Plate and the North American Plate. The Central Belt of the FRC is known as a the classic 'jadeite–glaucophane' type high-pressure and low-temperature metamorphic belts (Ernst, 1970; Terabayashi and Maruyama, 1998). It is a metamorphosed accretionary complex that formed from Late Jurassic to Miocene Pleistocene (Dumitru et al., 2015; Ernst, 1970). Most Franciscan rocks underwent low-temperature blueschist-facies metamorphism and very low-grade metamorphism at prehnite–pumpellyite or zeolite-facies condition. However, blocks of high-grade metamorphic rocks (coarse-grained garnet-bearing blueschist, eclogite, and rare garnet amphibolite), embedded within shale-matric and serpentinite-matrix mélanges, have also been described in the Franciscan Complex (e.g., Coleman and Lanphere, 1971; Krogh et al., 1994; Tsujimori et al., 2006, 2007; Wakabayashi, 1990). The CRO has been considered as a basement for the overlying the Great Valley Group deposits; it consists of serpentinized peridotites with a minor amount of gabbroic and basaltic rocks without mineralogical evidence of a high-pressure metamorphism (e.g., Coleman, 2000; Sherivais et al., 2005; Wakabayashi, 2017). The CRO rocks are locally disrupted by the movement of the San Andreas Fault. Consequently, serpentinites are ubiquitous in the FRC and some serpentinites could have derived from the CRO.

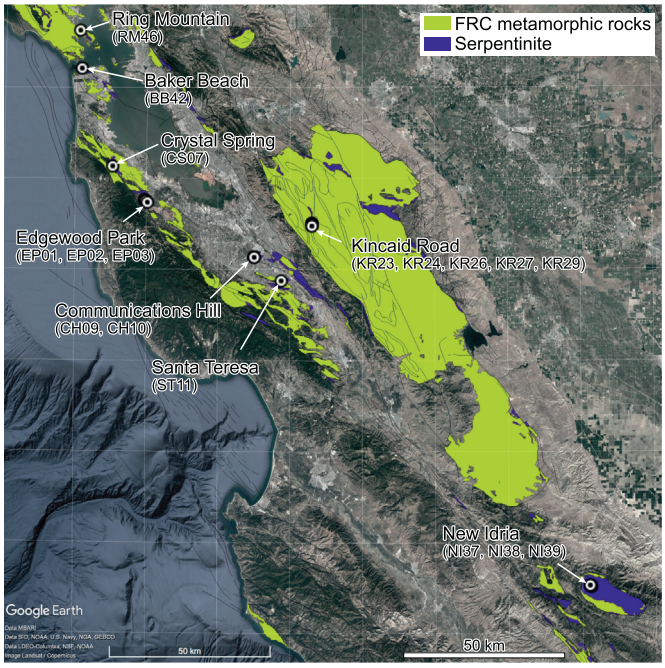

Fig. 1. A map showing sample localities and exposures of the Franciscan (FRC) metamorphic rocks and serpentinites. The base map was created using GoogleEarth and the USGS's California geologic map data (https://mrdata.usgs.gov/geology/state/state.php?state=CA).

In this study, we investigated serpentinites of the FRC in Ring Mountain (RM), Baker Beach (BB), Communications Hill (CH), Santa Teresa (ST), Crystal Spring (CS), Edgewood Park (EP), Kincaid Road (KR) and New Idria (NI) (Fig. 1).

3. Method

3.1. Sample preparation

Five thick polished rectangular plates of individual samples are bundled into one composite chip (about 25 mm long × 20 mm width × 5 mm thick) and mounted using a minimum amount of epoxy resin (Struers Specifix-40) to avoid boron contamination from epoxy resin. We prepared a total of four composite chips (20 samples), and made petrographical thin-sections and polished mounts from the composite chips. The polished mounts for isotope analyses were cleaned with milli-Q water in an ultrasonic bath.

3.2. Analytical procedure

Table 1 summarizes locations, lithological association and serpentine mineralogy of the studied serpentinites. Representative textures are shown in Figs. 2 and 3. The back-scattered electron (BSE) imaging was performed using a JEOL JSM-7001F field emission-scanning electron microscope (FE-SEM) at Tohoku University. The operation was performed at 15 kV acceleration voltage and 3.0 nA beam current. Identification of serpentine minerals was undertaken by a Horiba XploRA PLUS Confocal Raman Microscope at Tohoku University. A 532 nm solid-state Nd-YAG laser with 10 mW power was used as the light source.

Major element compositions of serpentinine minerals were analyzed in the polished thick section prepared for ablation volume correction (AVC) LA-MC-ICPMS (see below) near the laser-ablation craters after B isotope analyses (Fig. 4). An Oxford Instruments INCA energy

Table 1
List of samples showing localities, occurrence, modal volume of serpentine, type of serpentine mineral, and relict minerals.

Sample	Area	BS	Serp., vol%	Serp.	Relict minerals
RM46	Ring Mountain	no	91	Lz/Ctl	Ol, Opx, Cpx, Chr (Cr#41)
BB42	Baker Beach	no	86	Lz/Ctl	Ol, Opx, Cpx, Chr (Cr#46)
CH09	Communication Hil	no	90	Lz/Ctl	–
CH10	Communication Hil	no	76	Lz/Ctl	Opx,Chr (Cr#23)
ST11	Santa Teresa	no	88	Lz/Ctl	Ol, Opx, Cpx, Chr (Cr#33)
EP01	Edgewood Park	no	86	Lz/Ctl	Chr (Cr#37)
EP02	Edgewood Park	no	65	Lz/Ctl	Chr (Cr#26)
EP03	Edgewood Park	yes	79	Lz/Ctl	Ol, Opx, Cpx, Chr (Cr#28)
CS07	Crystal Spring	yes	87	Lz/Ctl	–
KR23	Kincaid Road	yes	91	Lz/Ctl	–
KR24	Kincaid Road	yes	85	Lz/Ctl	Opx, Cpx
KR26	Kincaid Road	yes	85	Lz/Ctl	Opx
KR27	Kincaid Road	yes	40	Atg	Ol, Opx, Cpx
KR29	Kincaid Road	yes	89	Lz/Ctl	Chr (Cr#78)
NI37	New Idria	yes	97	Atg	Cpx
NI38	New Idria	yes	95	Atg	–
NI39	New Idria	yes	96	Atg	Chr (Cr#64)

Lz/Ctl—lizardite or chrysotile, Atg—antigorite or antigorite + lizardite.
Serp., vol%—modal volume of serpentine.
Ol–olivine, Opx—orthopyroxene, Cpx—clinopyroxene, Chr—Chromian spinel/chromite.
BS—association of blueschist-facies metamorphic rocks.

dispersive electron microanalyzer system equipped with the JEOL JSM-7001F FE-SEM at Tohoku University was used with the same analytical condition given above.

The Raman spectra were measured ranging from 199.6 to 1194 cm^{-1} in 1.1 cm^{-1} steps (2400 g/mm). The measuring area was ~2 μm in diameter; the exposure time was 50 s. The Raman shift was calibrated using a reference silicon.

The modal abundance of serpentine minerals, i.e., degree of serpentinization, of each sample was quantitatively estimated by digital optical image processing of petrographic thin sections.

Boron isotope ratios ($^{11}B/^{10}B$) were determined by a LA-MC-ICPMS at the Japan Agency for Marine-Earth Science and Technology (JAMSTEC). The analyses were performed using an OK Laboratory OK-EX2000 (OK Lab, Tokyo, Japan) 193-nm excimer laser ablation system with at a ~20 ns pulse duration at repetition rate of 5 Hz. The 193ExLA was coupled to a modified Neptune (ThermoFisher Scientific, Bremen, Germany) MC-ICPMS. The spot diameter used was 200 μm and ~40 μm depth crater was generated after single spot analysis (Fig. 4). Mass bias correction was carried out by standard-sample bracketing method using the SRM 612 synthetic glass ($^{11}B/^{10}B = 4.042$; Jochum and Stoll, 2008) provided by the National Institute of Standard and Technology (NIST). An unknown sample measurement was corrected for by using a set of standard measurements made immediately before and after an unknown. Error propagation from the two standard measurements was also considered. The measured $^{11}B/^{10}B$ isotope ratios are expressed by $\delta^{11}B$ relative to the NIST SRM951 (boric acid) where $\delta^{11}B = [(^{11}B/^{10}B)_{Sample}/(^{11}B/^{10}B)_{SMR951}-1] \times 1000$ which was determined relative to SRM 612 of $\delta^{11}B = -0.25$ (Ishikawa and Tera, 1997). Residual analytical bias was present due to different sampling efficiencies between SRM 612 and the serpentine samples, which led to different aerosol mass loading to the ICP. The residual bias was corrected for following the ablation volume correction (AVC) method described by Kimura et al. (2016) which enabled accurate B isotope ratio analyses of various materials with different matrix. The volume of crater after B isotope measurement was measured with a digital microscope VHS-5000 (Keyence Co., Osaka, Japan) and used to correct for the residual bias. The bias factor during the analyses was constantly +0.5‰ for all the measured $\delta^{11}B$. Because the crater volumes were precisely measured, quantification of boron abundances from the same craters was simultaneously available with the determinations of $\delta^{11}B$ using the reference concentration $B = 34.3\ \mu g \cdot g^{-1}$ in SRM 612 (Jochum et al., 2005). For the analytical details see Kimura et al. (2016).

4. Sample descriptions

In our petrographic description, we use a term 'serpentinite' for serpentine-dominant ultramafic rocks without texture of original mantle peridotite. Instead, we use a term 'serpentinized peridotite' to describe the rocks still preserving original peridotite texture.

Ring Mountain sample (RM46) comes from a serpentinized harzburgite body that structurally overlies the Franciscan jadeite-bearing metagraywackes. Bero (2014) considered that this serpentinite body is a tectonic klippe possibly a fragment of the CRO. The samples are strongly serpentinized (91 vol% lizardite), but preserve relict olivine (Fo_{91}), orthopyroxene (2.5 wt% Al_2O_3), clinopyroxene (2.4 wt% Al_2O_3), and chromian spinel (Cr# [$= 100 \times Cr/(Cr + Al)$] = 41) (Fig. 2a).

Baker Beach sample (BB42), collected in a massive serpentinized harzburgite at Baker Beach (Wakabayashi, 2004), is highly serpentinized (56 vol% lizardite), preserving relict olivine (Fo_{91}), orthopyroxene (1.7 wt% Al_2O_3), clinopyroxene (2.2 wt% Al_2O_3), and chromian spinel (Cr# = 46) (Figs. 2b and 3a).

Communications Hill samples (CH09 and CH10) were collected from a massive serpentinized harzburgite body, which has been considered as a flat sheet of the CRO (Page et al., 1999). CH09 is a weakly sheared, pale-greenish serpentinite. It consists mainly chrysotile serpentine (90 vol%) with minor amount of chlorite and talc. CH10 is a grayish color serpentinite consisting of lizardite serpentinite (76 vol%). It preserves relict chromian spinel (Cr# = 23); talc veins and bastite after orthopyroxene are common (Fig. 2c).

Santa Teresa sample (ST11), was taken from a massive serpentinized peridotite body. The sample is highly serpentinized (88 vol% serpentine) but contains olivine (Fo_{91}), orthopyroxene (2.6 wt% Al_2O_3), clinopyroxene (2.3 wt% Al_2O_3), and chromian spinel (Cr# = 33) (Figs. 2d and 3b).

Edgewood Park samples (EP01, EP02 and EP03) come from mélange-like serpentinite along the highway I-280 (Uno and Kriby, 2019). EP02 is a massive serpentine boulder, located the side of the highway, near a serpentine exposure. All samples are massive serpentinized peridotite within a sheared serpentinite matrix. They consist mainly of lizardite and chrysotile serpentines with relict chromian spinel. Mesh texture after olivine and bastite texture after orthopyroxene are common (Figs. 2f, 3c and d); talc veins cut the serpentine matrix (Fig. 2e). Modal abundance of serpentine varies from 65 to 86 vol%. EP03 preserves relict olivine (Fo_{91}), orthopyroxene (2.9 wt% Al_2O_3), clinopyroxene (2.4 wt% Al_2O_3), and chromian spinel (Cr# = 28). The Cr#s of chromian spinel in EP01 and EP02 are 38 and 26, respectively.

Crystal Spring sample (CS07) was collected from an outcrop of serpentinite mélange near the San Andreas Fault. The serpentinite exposure contains tectonic blocks of Franciscan metagraywackes. The sample is a dark-colored serpentinite consisting of chrysotile serpentine with minor amount of chlorite, talc and magnetite. No relict mantle minerals remain in this sample, but mesh texture is common; modal abundance of serpentine is 87 vol% (Fig. 2g).

Kincaid Road samples (KR23, KR24, KR26, KR27 and KR29) were collected from an elongated serpentinite lenses associated within the Franciscan jadeite-bearing metagraywacke in Mt. Hamilton area (Blake and Wentworth, 1999). KR24 and KR27 are serpentinized peridotite with original granoblastic texture. KR27 preserves abundant relict olivine (Fo_{90}), orthopyroxene (3.6 wt% Al_2O_3) and clinopyroxene (3.7 wt% Al_2O_3) in antigorite-lizardite mixed serpentine (~40 vol%) (Fig. 3e). KR24 has relict clinopyroxene (3.1 wt% Al_2O_3). KR23, KR26 and KR29 are greenish serpentinite characterized by lizardite and chrysotile (Fig. 2h). Mesh texture of lizardite and chrysotile after olivine is common. Modal abundance of serpentine varies from ~85 to 91 vol%. Relict chromian spinels in Kincaid Road serpentinites are mostly replaced by magnetite and original composition (Cr# = 78) is only confirmed in KR29. The geologic occurrence indicates that the Kincaid Road serpentinites underwent a blueschist-facies metamorphism together with surrounding jadeite-bearing metagraywackes.

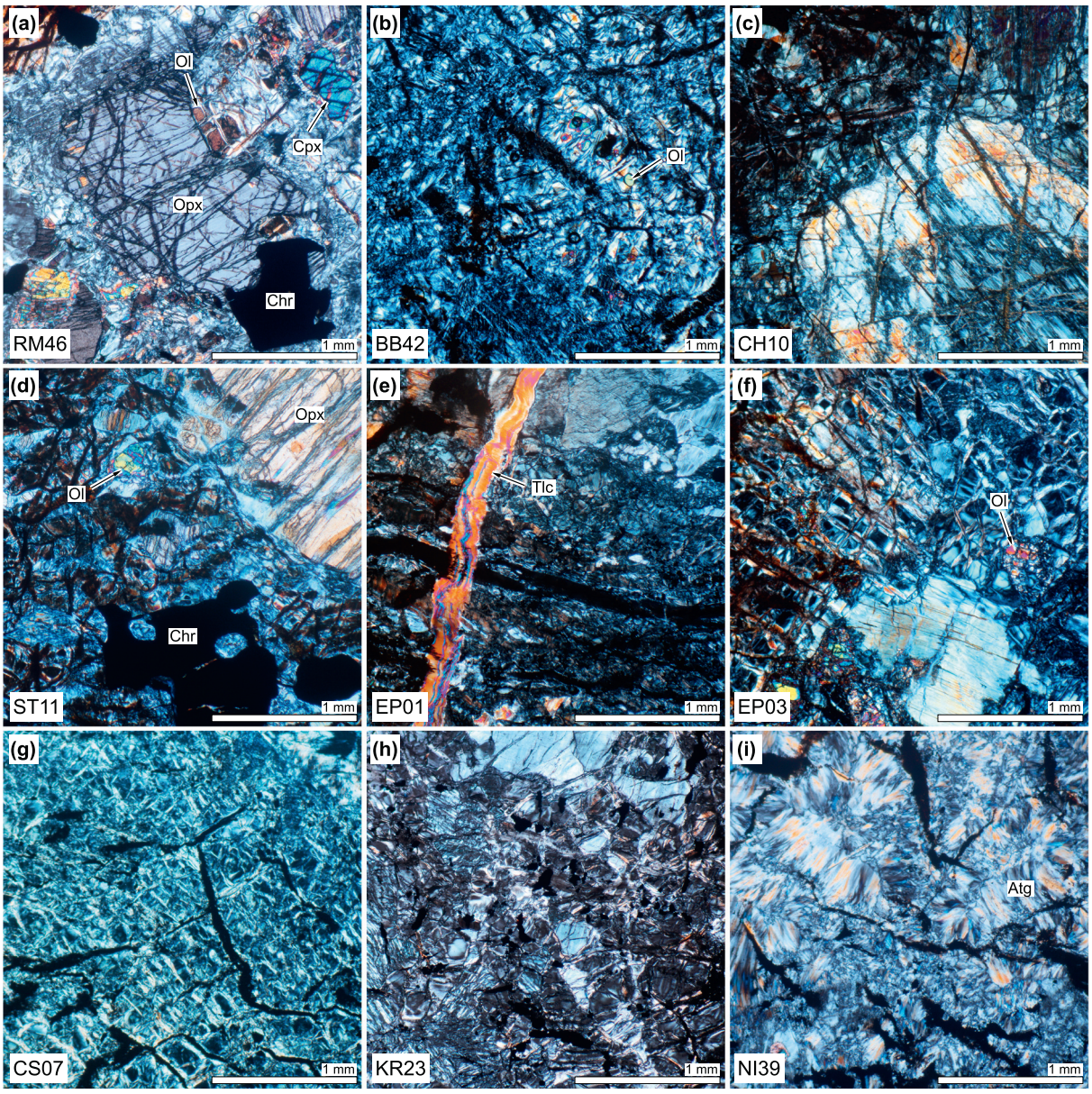

Fig. 2. Representative microtextures (cross-polarized photomicrographs) of the studied serpentinites. Scale bars represent 1 mm. All minerals without a label are serpentines. (a) Ring Mountain sample (RM46) preserving relict olivine (Ol), clinopyroxene (Cpx), orthopyroxene (Opx) and chromian spinel (Chr). (b) Baker Beach sample (BB42) preserving a minor relict olivine. (c) Communications Hill sample (CH10) showing bastite texture after orthopyroxene. (d) Santa Teresa sample (ST11) preserving peridotite minerals and textures. (e) Edgewood Park sample (EP01) containing a talc vein. (f) Edgewood Park sample (EP03) with minor relict minerals. (g) Crystal Spring sample (CS07) showing mesh texture after olivine. (h) Kincaid Road sample (KR23) showing bastite texture after orthopyroxene. (i) New Idria sample (NI39) showing antigorite-dominant matrix.

New Idria samples (NI37, NI38 and NI39) are antigorite serpentinite near the New Idria jadeite locality (Coleman, 1961; Takahashi et al., 2017, 2018). They are dark-greenish antigorite serpentinites with brucite, chlorite and rare secondary chrysotile (Figs. 2i and 3f). NI39 contains relict chromian spinel (Cr# = 64) and NI37 preserves relict clinopyroxene (1.7 wt% Al_2O_3). The modal abundance of serpentine varies from 95 to 97 vol%. The New Idria serpentinite is recognized as an on-land analogue of an active serpentinite diapir similar to the Izu–Bonin–Mariana forearc (Coleman, 1996; Tsujimori et al., 2007). The occurrence of jadeitite as well as blueschist, retrograde eclogite and garnet amphibolites suggest that the serpentinites underwent high-pressure metamorphism (Tsujimori et al., 2007). The occurrence of antigorite + brucite mineral assemblage in some serpentinites supports this idea.

4.1. Serpentine composition

The results are plotted in Al versus X_{Mg} [Mg/(Mg + Fe) atomic ratio] diagram (Fig. 5). Most serpentinites are characterized by low Al (<0.5 a.p.f.u.) and the X_{Mg} are mostly ranging from 0.88 to 0.96. Serpentinite pseudomorph after orthopyroxene tends to be Al-rich. Correlation between serpentinite composition and boron isotope was no observed.

5. Isotopic and elemental variations of boron

Table 2 shows the 51 spot analyses for 17 samples from 8 localities. Boron concentration and $\delta^{11}B$ among the samples vary widely, ranging from 1.6 to 239 $\mu g \cdot g^{-1}$ and − 12.0 to +24.4‰ (Fig. 6). The Ring Mountain serpentinite (RM46) shows moderate boron concentration (50–80

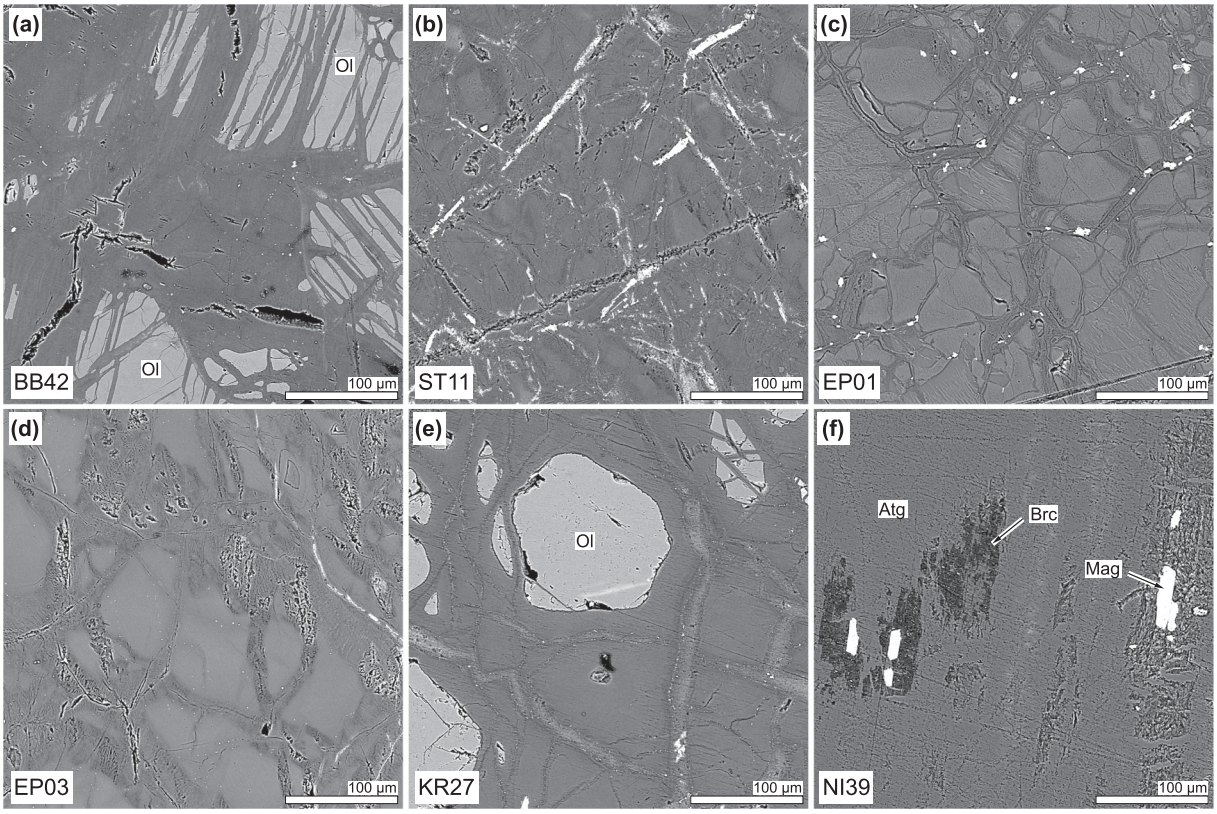

Fig. 3. Representative microtextures of the studied serpentinites shown by the back-scattered electron scanning electron microscopic images. Scale bars represent 100 μm. All minerals without a label are serpentines. Mesh texture after olivine: (a) Baker Beach sample (BB42), (b) Santa Teresa sample (ST11), (c) Edgewood Park sample (EP01), (d) Edgewood Park sample (EP03), (e) Kincaid Road sample (KR27). (f) Coexistence of brucite (Brc) and antigorite (Atg) in New Idria sample (NI39).

$\mu g \cdot g^{-1}$) and moderate to high $\delta^{11}B$ (+7.2 to +17.5‰). The Baker Beach serpentinite (BB42) also shows moderate boron (34–53 $\mu g \cdot g^{-1}$) and high $\delta^{11}B$ of +15.3 to +20.5‰. The Communications Hill serpentinites (CH09 and CH10) contain moderate boron (15–70 $\mu g \cdot g^{-1}$) and high $\delta^{11}B$ (+14.0 to +20.0‰). The Santa Teresa serpentinite (ST11) contains high boron (76–142 $\mu g \cdot g^{-1}$) and high $\delta^{11}B$ (+14.8 to +16.7‰). We identified two groups at the Edgewood Park serpentinites (EP01, EP02 and EP03): (1) EP01 and EP02 are characterized by very high boron (56–239 $\mu g \cdot g^{-1}$) and high $\delta^{11}B$ (+17.3 to +24.4‰). In contrast, (2) EP03 shows low boron (20–26 $\mu g \cdot g^{-1}$) and moderate $\delta^{11}B$ (+0.6 to +7.8‰). The Crystal Spring sample (CS07) is characterized by low boron (16–23 $\mu g \cdot g^{-1}$) and low $\delta^{11}B$ (+1.2 to +3.9‰). The Kincaid Road serpentinites (KR23, KR24, KR26, KR27 and KR29) are characterized by low to moderate boron (1.6–56 $\mu g \cdot g^{-1}$) and low to moderate $\delta^{11}B$ (−12.0 to +8.5‰). The New Idria serpentinites (NI37, NI38 and NI39) are also characterized by low boron (3–33 $\mu g \cdot g^{-1}$) and low $\delta^{11}B$ (−4.0 to +8.8‰). In particular, NI38 yields very low $\delta^{11}B$ of −4.0‰.

6. Discussion

6.1. Boron isotope composition of the Franciscan serpentinites

In-situ analysis offers the advantage of collecting data after petrographic observations. Although serpentinites have simple mineralogy, it has been known that the texture of serpentinites is variable (Figs. 2 and 3). In this study, we performed in-situ isotope analysis after spot selection based on serpentine texture and color. Nevertheless, we could not observe any correlations among major element, boron concentration, B isotope value, color, and texture (see an example in Fig. 5 for major elements and B isotopes). Polymorphs of serpentine minerals are divided into low-temperature type (< ~300 °C) lizardite (or chrysotile) and high-temperature type (~300–650 °C) antigorite (e.g., Evans, 2004). As mentioned above, New Idria samples are antigorite-bearing serpentinites and some Kincaid Road samples also contain both antigorite and lizardite. However, isotopic difference was not observed among serpentinites with different serpentine mineralogy from the same locality.

As shown in Fig. 6a, there are significant isotopic variations among sample localities. We grouped the isotopic composition of boron based on the presence and absence of associated blueschist-facies metamorphic rocks (Fig. 6). Serpentinites (including serpentinized peridotite) associated with the blueschist-facies metamorphic rocks are characterized by lighter boron (−12.0 to +8.8‰) than those of blueschist-absent rocks (+7.2 to +24.4‰) (Fig. 6). Note that serpentinites from the Kincaid Road of Mt. Hamilton area are enclosed within jadeite-bearing metagraywackes together with blocks of eclogite and garnet blueschist; those from the New Idria antigorite serpentinite also contains tectonic blocks of jadeitite, retrograde eclogite, and lawsonite blueschist. In the Edgewood Park, serpentinite (EP03) from an outcrop with a lawsonite-blueschist block shows significantly lower $\delta^{11}B$ than two other samples without blueschists. The lower $\delta^{11}B$ can be explained by Rayleigh fractionation, where by $\delta^{11}B$ decreases with increasing slab depth (e.g. Peacock and Hervig, 1999). In fact, SIMS boron isotope study of silicate minerals in blueschist clasts from Mariana serpentine seamount showed negative $\delta^{11}B$ value (−6.0 ± 4‰; Pabst et al., 2012), which is lower than the average value of altered oceanic crust (+3.4‰; Smith et al., 1995). Therefore, the geologic occurrence evokes that the lighter boron would be linked to fluid-mediated processes at 'jadeite–glaucophane' type blueschist-forming-depth (> ~1 GPa; e.g. Tsujimori and Ernst, 2014) or even deeper eclogite-forming depth (> ~2 GPa; e.g., Hacker et al., 2003). Conversely, the higher $\delta^{11}B$ values of blueschists-absent serpentinites suggest that serpentinization occurred at shallow depth by fluids with heavy ^{11}B such as seawater

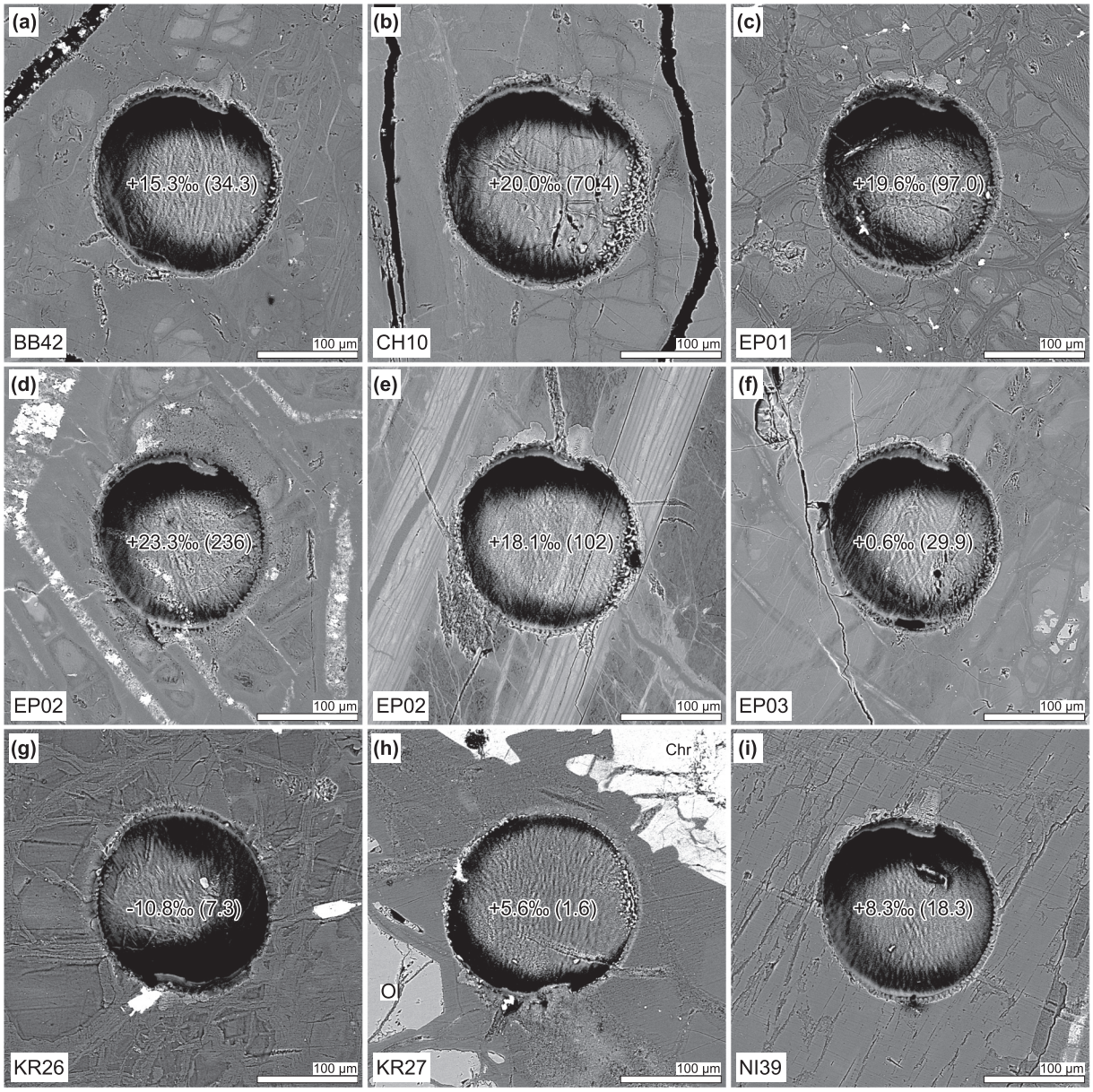

Fig. 4. Back-scattered electron images of representative laser ablation craters. Boron isotope values are shown in the craters with numbers in parentheses for boron concentrations in μg·g^{-1}. Scale bars represent 100 μm. The crater diameters are ~200 μm.

(+39.5‰; Spivack and Edmond, 1987), sedimentary pore fluids (e.g. +27.8 to +37.8‰; James and Palmer, 2000), or fluids from mud volcano (+22.5 to +39.2‰; Kopf et al., 2003). For example, serpentinites from the Mariana serpentinite seamount have heavier boron isotopic composition (+5.3 to +25.3‰) due to interaction with seawater and/or shallow pore fluids (Benton et al., 2001).

Martin et al. (2016) showed a similar result that mélange-forming antigorite serpentinites in the Motagua Mélange (Guatemala), with eclogite and jadeitite, have low δ^{11}B (−14.4 to +9.7‰). In contrast, they showed heavy boron isotopes (0 to +18.0‰) from ophiolite serpentinites without high-pressure metamorphic rocks. Martin et al. (2016) claim that boron isotope signature can discriminate the tectonic origin of serpentinites in Pacific-type orogenic belts. Our study also supports and reinforces such an idea.

6.2. Implications for sub-forearc serpentinites

The Cr# of chromian spinel (or chromite) in residual mantle peridotite is a robust petrogenetic indicator of the degree of partial melting (e.g., Arai, 1994; Dick and Bullen, 1984). In general, a forearc mantle is thought to be highly depleted in melt due to prior melting of the mantle peridotite either at mid-ocean ridges or supra-subduction zones (e.g., Davidson, 1996; Pearson et al., 2007). However, the chemical variations of chromian spinel in forearc mantle materials show various degree of partial melting as shown by those from the Mariana forearc (Cr# 40–81; e.g., Parkinson and Pearce, 1998). This indicates that the petrologic characteristics of the forearc mantle wedge are not always depleted.

The Franciscan serpentinites also show a wide variation of Cr# in chromian spinel (e.g., Barnes et al., 2013; Choi et al., 2008; Hirauchi et al., 2008, Uno and Kriby, 2019). For example, Hirauchi et al. (2008) studied serpentinized lherzolites with very low Cr# (11−13) of spinel from Jade Cove, near Big Sur, and suggested a possible tectonic setting as oceanic fracture zone near slow- to ultraslow-spreading center. However, they also suggested that the fertile abyssal peridotite have experienced an amphibolite-facies metamorphic event along slab-mantle interface within the subduction zone before the incorporation into the Franciscan Complex. Choi et al. (2008) studied depleted and very

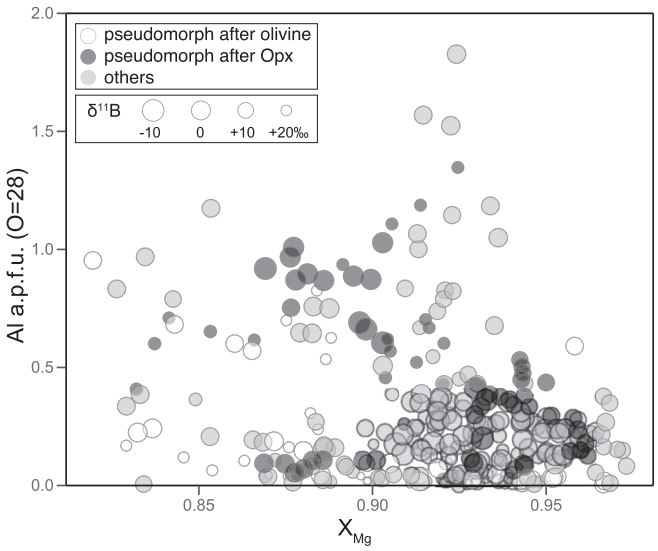

Fig. 5. Compositional variations of serpentinite in the studied samples. $\delta^{11}B$ values are expressed as size of the circles. The legend 'others' represent serpentines without any primary textures. See details of grouping in the text.

depleted harzburgitic lithology with high Cr# (59–84) chromite from Cuesta Ridge, near San Luis Obispo. They provided geochemical constraints that the harzburgite represented supra-subduction zone mantle.

In this study, we found relict chromian spinels, as strong resistance to serpentinization, some sample localities (Ring Mountain, Baker Beach, Communications Hill, Santa Teresa, Edgewood Park, Kincaid Road and New Idria). We confirmed the large variation of Cr#, ranging from 20 to 78 (Fig. 8). Our observations confirmed a trend that serpentinites without blueschist contain low Cr# spinel, suggesting a 'fertile' nature of residual mantle peridotite. These serpentinites are characterized by higher $\delta^{11}B$ (Fig. 8b). However, the mantle fertility estimated from Cr# does not necessarily correlate with the blueschist-facies rocks and boron isotope composition. More importantly, our data clearly discriminates two groups of serpentinites in the Franciscan Complex by the boron isotope composition. Those differences are supported by geologic occurrences defined by the presence or absence of blueschist-facies metamorphic rocks. The apparent correlation between mantle fertility versus boron isotope indicates a possibility that fertile peridotites remained in shallow part of forearc region where heavy ^{11}B is active. Antigorite-free serpentine mineralogy in higher $\delta^{11}B$ group also supports that these serpentinites formed in shallow environments (< 300 °C; e.g. Evans, 2004; Schwartz et al., 2013).

6.3. ABS model for boron isotope

Konrad-Schmolke and Halama (2014) model boron concentrations and isotope compositions in fluids released by a subducting slab during dehydration. Their model also shows that boron concentration and $\delta^{11}B$ of slab fluids decrease with increasing depth in the forearc region. We have calculated boron abundance and boron isotope compositions for residual slab materials and released slab fluids during subduction of an oceanic plate (Fig. 7). The model calculations were made using Arc Basalt Simulator version 3 (ABS3) code (Kimura et al., 2010) in combination with a temperature-dependent isotopic fractionation model for boron formulated by Wunder et al. (2005). Mineral-fluid partition coefficients for boron were assumed to be similar to those for Nb (Ishikawa and Tera, 1997). The effect of minor mineral phases, such as tourmaline, were not considered. The modified ABS3 model calculated dehydration profiles of the altered igneous oceanic crust (AOC) and sediment (SED) layers and hydration-dehydration profile of mantle wedge depleted peridotite (DMM) along a slab geotherm from 0.5–3.0 GPa. We assumed the following in the model calculations: the slab geotherm follows that of the Izu subduction system from Syracuse et al. (2010); boron abundances in the AOC, SED, and DMM were assumed as B = 1, 100, and 0.1 $\mu g \cdot g^{-1}$ with $\delta^{11}B = +10, +2$, and 0‰, respectively from Wunder et al. (2005); proportional contributions of AOC and SED fluids to DMM were at AOC: SED = 3: 7. Dehydration profiles and mineralogic modes of the AOC, SED, and DMM layers were calculated based on Perple_X thermodynamic model of Connolly and Kerrick (1987) with trace element partition coefficients between minerals and fluids compiled by Kimura et al. (2009).

Fig. 7a shows H_2O abundance in each layer. The total decrease of H_2O at given step in pressure corresponds to the fluid released. Rapid release of slab fluid occurs at 2.5–3.0 GPa. Boron abundances in the released

Table 2
Boron isotope compositions of the studied serpentinites.

Sample_#spot ID	Area	B, $\mu g \cdot g^{-1}$	2σ	$\delta^{11}B$	2σ	texture
RM46_#01	Ring Mountain	49.5	2.6	+7.2	0.6	–
RM46_#02	Ring Mountain	80.1	3.6	+13.6	0.6	–
RM46_#03	Ring Mountain	64.5	1.9	+17.5	0.6	–
BB42_#04	Baker Beach	53.1	0.9	+20.5	0.5	–
BB42_#05	Baker Beach	49.5	3.1	+18.3	0.5	–
BB42_#06	Baker Beach	34.3	1.5	+15.3	0.5	–
CH09_#07	Communications Hill	19.0	1.0	+14.3	0.5	–
CH09_#08	Communications Hill	14.7	0.7	+14.0	0.6	–
CH10_#09	Communications Hill	70.4	1.5	+20.0	0.4	psdm (Ol)
ST11_#10	Santa Teresa	75.6	5.9	+16.7	0.5	–
ST11_#11	Santa Teresa	141.9	7.2	+16.6	0.4	–
ST11_#12	Santa Teresa	85.1	3.8	+14.8	0.4	–
EP01_#13	Edgewood Park	97.0	4.8	+19.6	0.5	psdm (Ol)
EP01_#14	Edgewood Park	56.2	6.3	+17.3	0.4	psdm (Opx)
EP01_#15	Edgewood Park	73.7	5.0	+18.7	0.4	psdm (Ol)
EP02_#16	Edgewood Park	102.0	5.2	+18.1	0.5	psdm (Opx)
EP02_#17	Edgewood Park	239.4	8.3	+24.4	0.4	psdm (Ol)
EP02_#18	Edgewood Park	236.1	13.7	+23.3	0.5	psdm (Ol)
EP03_#19	Edgewood Park	21.9	0.6	+0.6	0.5	psdm (Ol)
EP03_#20	Edgewood Park	26.1	2.4	+7.8	0.5	–
EP03_#21	Edgewood Park	19.7	1.1	+5.0	0.5	–
CS07_#22	Crystal Spring	22.6	0.8	+1.2	0.6	psdm (Opx)
CS07_#23	Crystal Spring	15.5	0.6	+3.9	4.4	–
KR23_#24	Kincaid Road	19.8	0.4	+7.5	0.6	–
KR23_#25	Kincaid Road	13.9	0.6	+4.5	0.6	psdm (Ol)
KR24_#26	Kincaid Road	7.8	0.2	−0.7	0.7	–
KR24_#27	Kincaid Road	10.2	1.1	−4.4	0.7	psdm (Opx)
KR24_#28	Kincaid Road	9.5	2.5	−3.8	0.8	–
KR26_#29	Kincaid Road	7.5	0.1	−12.0	0.7	–
KR26_#30	Kincaid Road	8.0	0.6	−4.9	0.7	–
KR26_#31	Kincaid Road	7.3	0.3	−10.8	0.8	psdm (Opx)
KR27_#32	Kincaid Road	1.6	0.2	+5.6	3.4	–
KR27_#33	Kincaid Road	11.4	0.6	+8.5	0.6	–
KR27_#34	Kincaid Road	2.5	0.2	+7.1	2.2	–
KR29_#35	Kincaid Road	55.5	2.1	+4.0	0.5	psdm (Opx)
KR29_#36	Kincaid Road	38.5	1.5	+4.9	0.5	psdm (Ol)
KR29_#37	Kincaid Road	32.0	1.1	+6.3	0.5	psdm (Ol)
NI37_#38	New Idria	13.5	0.7	−0.6	0.9	–
NI37_#39	New Idria	13.7	0.9	+5.0	0.8	psdm (Opx)
NI37_#40	New Idria	5.1	1.2	+1.7	1.4	–
NI37_#41	New Idria	15.9	1.0	+1.3	0.9	–
NI37_#42	New Idria	15.2	1.1	+1.2	0.9	–
NI38_#43	New Idria	12.2	0.7	+3.8	1.0	–
NI38_#44	New Idria	32.7	1.8	+5.2	0.8	psdm (Opx)
NI38_#45	New Idria	16.7	1.0	+6.7	0.8	psdm (Opx)
NI38_#46	New Idria	10.7	0.6	−4.0	0.8	–
NI38_#47	New Idria	18.3	1.4	+8.3	1.0	psdm (Opx)
NI39_#48	New Idria	3.0	0.4	+6.9	2.1	–
NI39_#49	New Idria	29.8	1.1	+4.5	1.1	–
NI39_#50	New Idria	15.3	0.7	+8.8	1.1	–
NI39_#51	New Idria	11.4	0.9	+8.0	1.2	–

Lz/Ctl—lizardite or chrysotile, Atg—antigorite or antigorite + lizardite.
psdm (Ol or Opx) —pseudomorph after olivine or orthopyroxene.

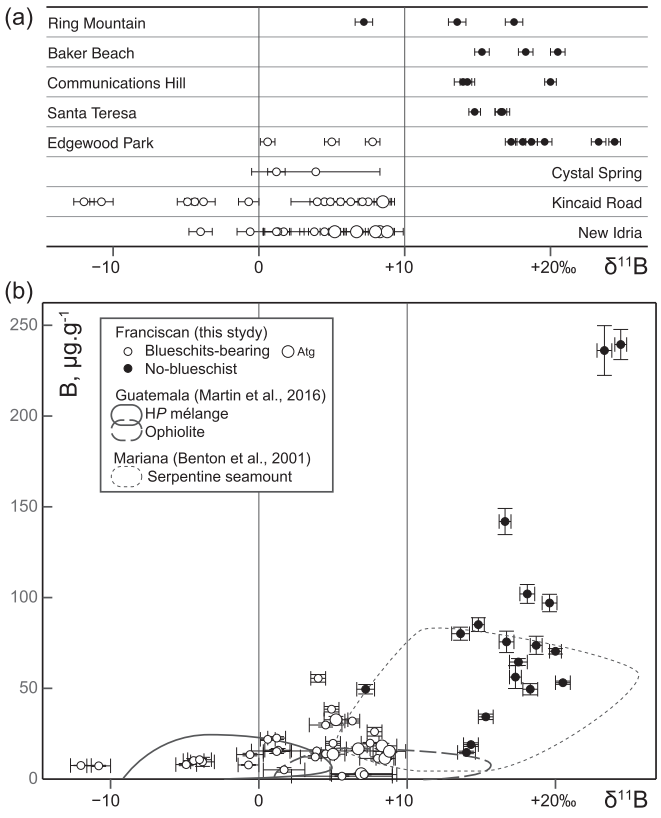

Fig. 6. Summary of $\delta^{11}B$ of the studied Franciscan serpentinites. (a) $\delta^{11}B$ grouped by areas. Note that white-circle symbols represent serpentinite associated with blueschist-facies metamorphic rocks. (b) $\delta^{11}B$ versus boron diagram showing compositional variations of the studied samples. For comparisons, compositional trend of serpentinites from the Motagua Suture Zone of Guatemala (Martin et al., 2016) and Mariana forearc (Benton et al., 2001) are also shown.

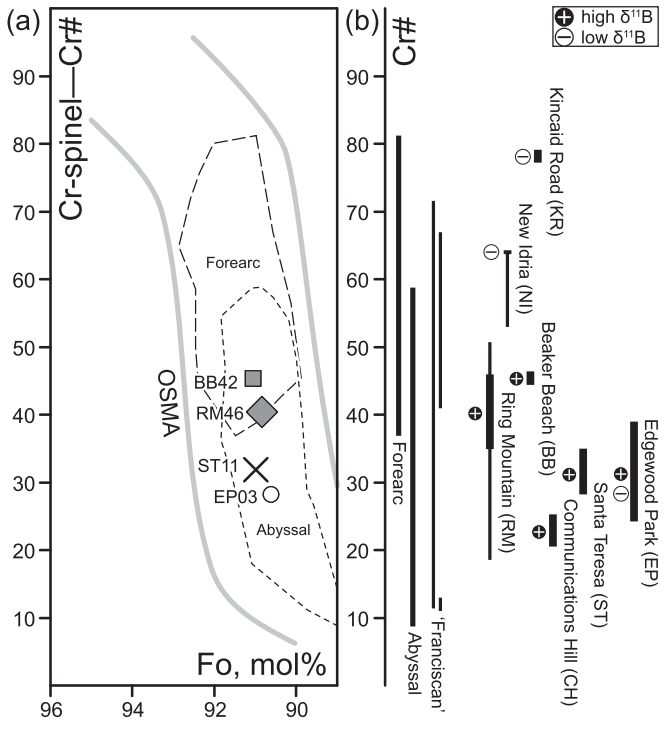

Fig. 8. Compositional features of relict minerals preserved in some samples. (a) Cr# [=Cr/(Cr + Al) × 100] versus forsterite component (Fo) of olivine diagram for relict olivine and coexisting chromian spinel. OSMA represents an olivine-spinel mantle array (Arai, 1994). Generalized ranges of forearc and abyssal peridotite are after Bloomer and Hawkins (1983), Dick and Bullen (1984), Bloomer and Fisher (1987), Ishii et al. (1992), Arai (1994), and Parkinson's and Pearce (1998). (b) Cr# of relict chromian spinels in samples from Kincaid Road, New Idria, Communications Hill and Edgewood Park. Two groups of Franciscan serpentinites are shown in rectangular areas with '+' (high $\delta^{11}B$) and '–' (low $\delta^{11}B$) symbols. The Cr#s of Franciscan (sensu *lato*) are after Hirauchi et al. (2008) and Barnes et al. (2013).

fluids remain almost constant at 300–400 $\mu g \cdot g^{-1}$ for SED, decrease from 49 to 4 $\mu g \cdot g^{-1}$ for AOC and from 8 to 1.5 $\mu g \cdot g^{-1}$ for DMM (Fig. 7b). The $\delta^{11}B$ in the residual slab layers decreased from +10 to −21‰ for AOC, +2 to −0.7‰ for SED, and 0 to −17‰ for DMM. Those for slab fluids also decreased from +37 to −14‰ for AOC, +29 to +6 for SED, and + 27 to −10‰ for DMM (Fig. 7c). The fluids from AOC, SED, and DMM layers are all possible candidates for the metasomatic fluids of the forearc serpentinites. Our analytical results fit well with calculated boron and $\delta^{11}B$ compositions from the depth range 2.5–3.0 GPa (400–750 °C) for the blueschist-present serpentinites and 0.5–2.0 GPa

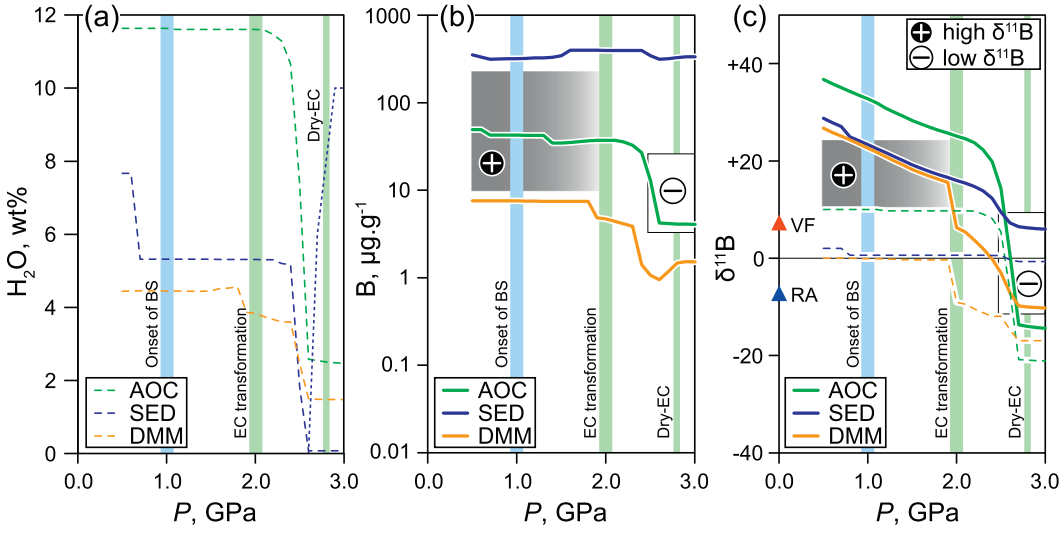

Fig. 7. ABS slab dehydration model. Systematic changes of boron abundance and $\delta^{11}B$ in the slab fluid are calculated using the Arc Basalt Simulator ver.3 (ABS3) model (Kimura et al., 2010); see details in the text. (a) Water abundances in each slab layer and amounts of released fluid. A blue hashed line represents melts from SED. Approximate depths of onset of blueschist (BS) and eclogite (EC) transformation are also shown in bold lines. (b) Boron abundance changes in slab fluids. Two groups of Franciscan serpentinites are shown in rectangular areas with '+' (high $\delta^{11}B$) and '–' (low $\delta^{11}B$) symbols. (c) $\delta^{11}B$ changes in slab fluids. Dashed lines represent $\delta^{11}B$ of residual sources (slabs). VF and RA represent $\delta^{11}B$ in the volcanic front and rear arc basalts. (For interpretation of the references to color in this figure legend, the reader is referred to the web version of this article.)

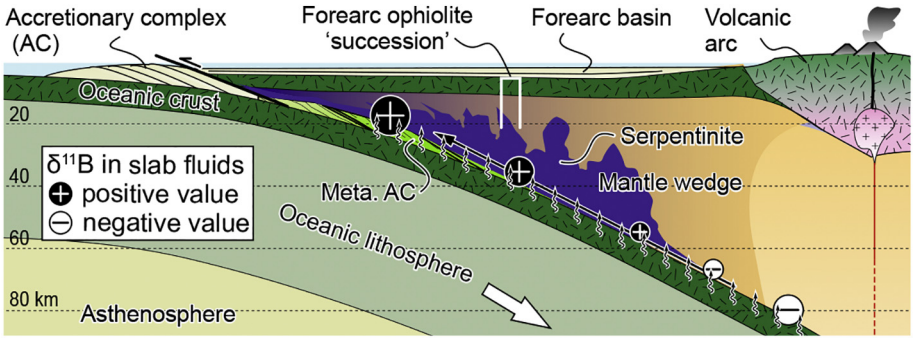

Fig. 9. A schematic cross section showing a subduction zone and the inferred boron isotope trends of dehydrating deep slab fluids. The relative size of '+' and '-' symbols indicates change of the $\delta^{11}B$ values; see details in text and Fig. 7. A bold arrow indicates buoyancy-induced flows of serpentinites from deeper portion.

(200–400 °C) for the blueschist-absent serpentinite groups, respectively (see rectangular boxes in Fig. 7b and c). The results are fairly consistent with the serpentinite mineralogy where antigorite (300–650 °C) and chrysotile/lizardite (< 300 °C) are major serpentine minerals, respectively. Presence of lawsonite blueschists and eclogites (< ~2.5 GPa, < ~450 °C; e.g., Tsujimori and Ernst, 2014; Hacker et al., 2003) in the former is also consistent with the *P–T* conditions of these particular fluid compositions of boron.

Considering the inferred evolution of boron isotope ratios in a subducting slab, sub-forearc serpentinites are likely affected by dehydrating deep slab fluids with light boron (Fig. 9). The boron concentrations are high for the serpentinites formed from low-temperature, heavier boron slab fluids, whereas concentrations are low in the serpentinites from high-temperature, lighter boron fluids. Such the scenario would be supported by both Martin et al. (2016) and this study. We propose that the blueschist-bearing and/or blueschist-associated serpentinites were affected by fluids released from subducting slab in the depth of > ~2 GPa and migrated upward (Fig. 7).

In-situ boron isotope geochemistry of serpentinites has the potential to provide better understanding of boron isotope systematics in subduction zone. This approach will eventually contribute to understanding the elemental mass balance of subduction systems by deciphering shallow-to-intermediate-depth forearc processes (0–2.0 GPa) which is rarely leached from the surface records.

7. Conclusion

Boron isotope study of Franciscan serpentinites using an ablation volume correction (AVC) LA-MC-ICPMS discriminates two groups. Serpentinites associated with blueschists (or enclosing blueschist blocks) are characterized by lighter boron isotope than serpentinites without blueschist-facies rocks. We interpret that lighter boron isotope signature of blueschist-bearing serpentinites results from interaction with forearc slab fluids with low $\delta^{11}B$ in deeper depth. The deep forearc slab fluids experience Rayleigh distillation and progressively released heavy ^{11}B during dehydration in shallow depth. In contrast, the blueschist-absent serpentinites with heavier boron isotope can be explained to have formed at shallow environment where fluids with heavy ^{11}B is active. Inferred $\delta^{11}B$ values of slab fluids from subducting slab by our ABS model fit the observations. This study supports an effectiveness of boron isotope composition for identification of the origin of serpentinites in Pacific-type orogenic belt.

Acknowledgements

We thank Steve Kirby and John Wakabayashi for their kind assistances for collecting serpentinite samples. We also thank Bob Coleman for his information about serpentinites in New Idria. This research was supported by the Center for Northeast Asian Studies, Tohoku University and the Japan Agency for Marine-Earth Science and Technology (JAMSTEC) in part by grants from the MEXT/JSPS KAKENHI JP15H05212 and JP18H01299 to T. Tsujimori and JP15H02148, JP16H01123, and JP18H04372 to J.-I. Kimura. The fieldwork was supported in part by the Collection Building Fellowship of the National Museum of Nature and Science, Tokyo; we thank Kenichiro Tani for this opportunity. We appreciate for constructive reviews from Céline Martin, Yuji Ichiyama, and an anonymous reviewer. We extend our appreciation to Ryosuke Oyanagi and Noriyoshi Tsuchiya for their assistance on the micro Raman spectroscopy. We also thank Daniel Pastor-Galán for feedback.

References

Arai, S., 1994. Characterization of spinel peridotites by olivine spinel compositional relationships: review and interpretation. Chemical Geology 113, 191–204.
Barnes, J.D., Eldam, R., Lee, A.C., Errico, J.C., Loewy, S., Cisneros, M., 2013. Petrogenesis of serpentinites from the Franciscan complex, western California, USA. Lithos 178, 143–157.
Benton, L.D., Ryan, J.G., Tera, F., 2001. Boron isotope systematics of slab fluids as inferred from a serpentine seamount Mariana forearc. Earth and Planetary Science Letters 187, 273–282.
Bero, D.A., 2014. Geology of Ring Mountain and Tiburon Peninsula, Marine Country. California. Geological Survey Map Sheet 62.
Blake, M.C., Wentworth, C.M., 1999. Structure and metamorphism of the Franciscan complex, Mt. Hamilton Area, Northern California. International Geology Review 42, 417–424.
Bloomer, S.H., Fisher, R.L., 1987. Petrology and geochemistry of igneous rocks from the Tonga Trench: a non-accreting plate boundary. Journal of Geology 95, 469–495.
Bloomer, S.H., Hawkins, J.W., 1983. Gabbroic and ultramafic rocks from the Mariana Trench: an island arc ophiolite. AGU Geophysical Monograph Series 27, 294–317.
Choi, S.H., Shervais, J.W., Mukasa, S.B., 2008. Supra-subduction and abyssal mantle peridotites of the Coast Range ophiolite, California. Contributions to Mineralogy and Petrology 156, 551–576.
Coleman, R.G., 1961. Jadeite deposits of the clear creek Area, New Idria district, San Benito Country, California. Journal of Petrology 2, 209–247.
Coleman, R.G., 1971. Plate tectonic emplacement of upper mantle peridotites along continental edges. Journal of Geophysical Research 76, 1212–1222.
Coleman, R.G., 1996. New Idria serpentinite: A land management dilemma. Environmental and Engineering Geoscience 2, 9–22.
Coleman, R.G., 2000. Prospecting for ophiolites along the California continental margin. Special Paper of the Geological Society of America 349, 351–364.
Coleman, R.G., Lanphere, M.A., 1971. Distribution and age of high-grade blueschist, associated eclogites, and amphibolites from Oregon and California. Geological Society of America Bulletin 82, 2397–2412.
Connolly, J.A.D., Kerrick, D.M., 1987. An algorithm and computer program for calculating composition phase diagram. Calphad 11, 1–55.
Davidson, J.P., 1996. Deciphering mantle and crustal signatures in subduction zone magmatism. Geophysical Monograph 96, 251–262.
Deschamps, F., Godard, M., Guillot, S., Hattori, K., 2013. Geochemistry of subduction zone serpentinites: a review. Lithos 178, 96–127.
Dewey, J.F., Bird, P., 1970. Mountain belts and the new global tectonics. Journal of Geophysics Research 75, 2625–2647.
Dick, H.J.B., Bullen, T., 1984. Chromian spinel as a petrogenetic indicator in abyssal and alpine-type peridotites and spatially associated lavas. Contributions to Mineralogy and Petrology 86, 56–76.
Dumitru, T.A., Ernst, W.G., Hourigan, J.K., Mclaughlin, R.J., 2015. Detrital zircon U-Pb reconnaissance of the Franciscan subduction complex in northwestern California. International Geology Review 57, 767–800.
Ernst, W.G., 1970. Tectonic contact between the Franciscan melange and the Great Valley sequence, crustal expression of a late Mesozoic Benioff zone. Journal of Geophysical Research 75, 886–901.

Ernst, W.G., 1975. Systematics of large-scale tectonics and age progressions in Alpine and Circum-Pacific blueschist belt. Tectonophysics 26, 229–246.
Ernst, W.G., 2017. Geologic evolution of a cretaceous tectonometamorphic unit in the Franciscan complex, western California. International Geology Review 59, 563–576.
Evans, B.W., 2004. The serpentinite multisystem revisited: Chrysotile is metastable. International Geology Review 46, 479–506.
Gerya, T.V., Stockhert, B., Perchuk, A.L., 2002. Exhumation of high-pressure metamorphic rocks in a subduction channel: a numerical simulation. Tectonics 21. https://doi.org/10.1029/2002TC001406.
Hacker, B.R., Abers, G.A., Peacock, S.M., 2003. Subduction factory 1. Theoretical mineralogy, densities, seismic wave speeds, and H_2O contents. Journal of Geophysical Research 108, B1:2029. https://doi.org/10.1029/2001JB001127.
Hirauchi, K., Tamura, A., Arai, S., Yamaguchi, H., Hisada, K., 2008. Fertile abyssal peridotites within the Franciscan subduction complex, Central California; possible origin as detached remnants of oceanic fracture zones located close to a slow-spreding ridge. Lithos 105, 319–328.
Ishii, T., Robinson, P.T., Maekawa, H., Fiske, R., 1992. Petrological studies of peridotites from diapiric serpentinite seamounts in the Izu-Ogasawara-Mariana forearc, Leg 125. Proceeding of the Ocean Drilling Program, Scientific Results 125, 445–485.
Ishikawa, T., Tera, F., 1997. Source, composition and distribution of the fluid in the Kurile mantle wedge: Constraints from across-arc variation of B/Nb and B isotope. Earth and Planetary Science Letters 152, 123–138.
James, R.H., Palmer, M.R., 2000. Marine geochemical cycles of the alkali elements and boron: the role of sediments. Geochemica et Cosmochimica Acta 64, 3111–3122.
Jochum, K.P., Stoll, B., 2008. Reference materials for elemental and isotopic analyses by La-(MC)-ICP-MS: Successes and outstanding needs. Mineralogical Association of Canada Short Course 40, 147–168.
Jochum, K.P., Nohl, U., Herwig, K., Lammel, E., Stoll, B., Hofmann, A.W., 2005. GeoReM: a New geochemical database for reference materials and isotopic standards. Geostandards and Geoanalytical Research 29, 333–338.
Kimura, J.-I., Hacker, B.R., van Keken, P.E., Kawabata, H., Yoshida, T., Stern, R.J., 2009. Arc Basalt Simulator version 2, a simulation for slab dehydration and fluid-fluxed mantle melting for arc basalts: Modeling scheme and application. Geochemistry, Geophysics, Geosystems 10, Q09004. https://doi.org/10.1029/2008GC002217.
Kimura, J.-I., Adam, J.R.K., Rowe, M., Nakano, N., Katakuse, M., van Keken, P., Hacker, B., Stern, R.J., 2010. Origin of cross-chain geochemical variation in Quaternary lavas from northern Izu arc: a quantitative mass balance approach on source identification and mantle wedge processes. Geochemistry, Geophysics, Geosystems 11, Q10011. https://doi.org/10.1029/2010GC003050.
Kimura, J., Chang, Q., Ishikawa, Tsujimori, T., 2016. Influence of laser parameters on isotope fractionation and optimization of lithium and boron isotope ratio measurements using laser ablation multiple Faraday collector-inductively coupled plasma mass spectrometry. Journal of Analytical Atomic Spectrometry 31, 2305–2320.
Konrad-Schmolke, M., Halama, R., 2014. Combined thermodynamic–geochemical modeling in metamorphic geology: boron as tracer of fluid–rock interaction. Lithos 208, 393–414.
Kopf, A., German, M., Deyhle, A., Frape, S., Hesse, R., 2003. Fluid geochemistry in the Japan trench forearc (ODP Leg 186): A synthesis. Proceedings of the Ocean Drilling Program Science Result 186, 1–23.
Krogh, E.J., Oh, C.W., Liou, J.C., 1994. Polyphase and anticlockwise P–T evolution for Franciscan eclogites and blueschist from Jenner, California, USA. Journal of Meramoephic Geology 12, 121–134.
Marschall, H.R., Altherr, R., Rupke, L., 2007. Squeezing out the slab–modelling the release of Li, be and B during progressive high-pressure metamorphism. Chemical Geology 239, 323–335.
Martin, C., Flores, K.E., Harlow, G.E., 2016. Boron isotopic discrimination for subduction-related serpentinites. Geology 44, 899–902.
Matsuda, T., Uyeda, S., 1971. On the Pacific-type orogeny and its model: Extention of the paired metamorphic belts concept and possible origin of marginal basins. Tectonophysics 11, 5–27.
Pabst, S., Zack, T., Savov, I.P., Ludwig, T., Rost, D., 2012. The fate of subducted oceanic slabs in the shallow mantle: Insights from boron isotopes and light elemnt composition of metasomatized blueschists from the Mariana forearc. Lithos 132-133, 162–179.
Page, B.M., De Vito, L.A., Coleman, R.G., 1999. Tectonic emplacement of serpentinite southeast of San Jose, California. International Geology Review 41, 494–565.
Parkinson, I.J., Pearce, J.A., 1998. Peridotites from the Izu-Bonin-Mariana forearc (ODP Leg 125): evidence for mantle melting and melt-mantle interaction in a supra-subduction zone setting. Journal of Petrology 39, 1577–1618.
Peacock, S.M., Hervig, R.L., 1999. Boron isotopic composition of subduction zone metamorphic rocks. Chemical Geology 160, 281–290.
Pearson, D.G., Parman, S.W., Nowell, N.G., 2007. A link between large mantle melting events and continent growth seen in osmium isotopes. Nature 449, 202–205.
Scambelluri, M., Tonarini, S., 2012. Boron isotope evidence for shallow fluid transfer across subduction zones by serpentinized mantle. Geology 40, 907–910.
Scambelluri, M., Fiebig, J., Malaspina, N., Muntener, O., Pettke, T., 2004. Serpentinite subduction: Implications for Fluid Processes and Trace-Element Recycling. International Geology Review 46, 595–613.
Schwartz, S., Guillot, S., Reynard, B., Lafay, R., Debret, B., Nicollet, C., Lanari, P., Auzende, A.L., 2013. Pressure-temperature estimates of the lizardite/antigorite transition in high pressure serpentinites. Lithos 178, 197–210.
Sherivais, J.W., Murehey, B.L., Kimbrough, D.L., Renne, P.R., Hanan, B., 2005. Radioisotopic and biostratigraphic age relations in the Coast Range Ophiolite, northern California: Implication for the tectonic evolution of the Western Cordillera. Bulletin of the Geological Society of America 117, 633–653.
Smith, H.J., Spivack, A.J., Staudigel, H., Hart, S.R., 1995. The boron isotopic composition of altered oceanic crust. Chemical Geology 126, 119–135.
Spivack, A.J., Edmond, J.M., 1987. Boron isotope exchange between seawater and the ocean crust. Geochimica et Cosmochimica Acta 126, 119–135.
Syracuse, E.M., van Keken, P.E., Abers, G.A., 2010. The global range of subduction zone thermal models. Physics of the Earth and Planetary Interiors 183, 73–90.
Takahashi, N., Tsujimori, T., Kayama, M., Nishido, H., 2017. Cathodoluminescence petrography of P-type jadeitites from the New Idria serpentinite body, California. Journal of Mineralogical and Petrological Sciences 112, 291–299.
Takahashi, N., Tsujimori, T., Chang, Q., Kimura, J.-I., 2018. In-situ lithium isotope geochemistry for a veined jadeitite from the New Idria serpentinite body, California: Constraints on slab-derived fluid and fluid-rock interaction. Lithos 318-319, 376–385.
Terabayashi, M., Maruyama, S., 1998. Large pressure gap between the Coastal and Central Franciscan belts, northern and Central California. Tectonophysics 285, 87–101.
Tsujimori, T., Ernst, W.G., 2014. Lawsonite blueschists and lawsonite eclogites as proxies for palaeo-subduction zone processes: a review. Journal of Metamorphic Geology 32, 437–454.
Tsujimori, T., Matsumoto, K., Wakabayashi, J., Liou, J.G., 2006. Franciscan eclogite revisited: Reevaluation of the P-T evolution of tectonic blocks form Tiburon Peninsula, California, U.S.A. Mineralogy and Petrology 88, 243–267.
Tsujimori, T., Liou, J.G., Coleman, R.G., 2007. Finding of high-grade tectonic blocks from the New Idria serpentinite body, Diablo Range, California: Petrologic constrains on the tectonic evolution of an active serpentine diapir. Geological Society of America Special Papers 419, 67–80.
Uno M., Kirby S., 2019. Evidence for multiple stages of serpentinization from the mantle through the crust in the Redwood City Serpentinite mélange along the San Andreas Fault in California. Lithos https://doi.org/10.1016/j.lithos.2019.02.005.
Wakabayashi, J., 1990. Counterclockwise P-T-t paths from amphibolites, Franciscan complex, California: Metamorphism during the early stages of subduction. Journal of Geology 98, 657–680.
Wakabayashi, J., 1999. Subduction and the rock record: Concepts developed in the Franciscan complex, California. Special Paper of the Geological Society of America 338, 123–133.
Wakabayashi, J., 2004. Contrasting setting of serpentinite bodies, San Francisco bay area, California: Derivation from the subducting plate vs. mantle hanging wall? International Geology Review 46, 1103–1118.
Wakabayashi, J, 2011. Mélanges of the Franciscan complex, California: diverse structureal settings, evidence for sedimentary mixing, and their connection to subduction processes. Geological Society of America Special Papers 480, 117–141.
Wakabayashi, J., 2012. Subducted sedimentary serpentinite mélanges: Record of multiple burial-exhumation cycles and subduction erosion. Tectonophysics 568-569, 230–247.
Wakabayashi, J., 2015. Anatomy of a subduction complex: architecture of the Franciscan complex, California, at multiple length and time scales. International Geology Review 57, 669–746.
Wakabayashi, J., 2017. Serpentinites and serpentinites: Variety of origins and emplacement mechanisms of serpentinite bodies in the California Cordillera. Island Arc 26, 1–14.
Wunder, B., Meixner, A., Romer, R.L., Wirth, R., Heinrich, W., 2005. The Geochemical cycle of boron: Constraints from boron isotope partitioning experiments between mica and fluid. Lithos 84, 206–216.